

UCLA

UCLA Previously Published Works

Title

Biallelic loss-of-function variants in CACHD1 cause a novel neurodevelopmental syndrome with facial dysmorphism and multisystem congenital abnormalities.

Permalink

<https://escholarship.org/uc/item/6f84r0p3>

Journal

Genetics in Medicine, 26(4)

Authors

Scala, Marcello

Khan, Kamal

Beneteau, Claire

et al.

Publication Date

2024-04-01

DOI

10.1016/j.gim.2023.101057

Peer reviewed



Published in final edited form as:

Genet Med. 2024 April ; 26(4): 101057. doi:10.1016/j.gim.2023.101057.

Biallelic loss-of-function variants in *CACHD1* cause a novel neurodevelopmental syndrome with facial dysmorphism and multisystem congenital abnormalities

Marcello Scala^{1,2,3,23}, Kamal Khan^{4,23}, Claire Beneteau^{5,6,7,23}, Rachel G. Fox⁸, Sandra von Hardenberg⁹, Ayaz Khan⁴, Madeleine Joubert^{6,10}, Lorraine Fievet¹¹, Marie Musquer^{6,10}, Claudine Le Vaillant¹², Julie Korda Holsclaw¹¹, Derek Lim^{13,14}, Ann-Cathrine Berking⁹, Andrea Accogli¹, Thea Giacomini^{1,15}, Lino Nobili^{1,15}, Pasquale Striano^{1,2}, Federico Zara^{1,3}, Annalaura Torella^{16,17}, Vincenzo Nigro^{16,17}, Benjamin Cogné^{5,18}, Max R. Salick¹⁹, Ajamete Kaykas¹⁹, Kevin Egan²⁰, Valeria Capra³, Stéphane Bézieau^{5,18}, Erica E. Davis^{4,21,24,*}, Michael F. Wells^{8,20,22,24,*}

*Correspondence: eridavis@luriechildrens.org (E.E.D.) and mfwells@mednet.ucla.edu (M.F.W.).

AUTHOR CONTRIBUTIONS

M.S. conceived the project in collaboration with K.K. and R.F. M.S. assembled the study cohort, performed genetic and clinical characterization, and delineated the genotype-phenotype spectrum. K.K. generated and characterized the molecular and morphological phenotype of *cachd1* zebrafish mutants. R.F. generated CRISPR-edited *CACHD1* cell lines and performed RNA sequencing. M.R.S. performed imaging and scRNA-seq experiments on neurospheres. C.B., S.v.H., A.K., M.J., L.F., M.M., C.L.V., J.K.H., D.L., A.B., A.A., T.G., L.N., P.S., F.Z., A.T., V.N., B.C., V.C., and S.B. participated in genetic investigations, clinical assessment, and data sharing; E.E.D. and M.F.W. supervised the project. M.S. wrote the first draft of the manuscript with inputs and revisions from K.K., R.F., E.E.D., and M.F.W.

CONFLICT OF INTEREST

The authors declare no conflicts of interest.

WEB RESOURCES

ACMG, <https://www.acmg.net/ACMG/Medical-Genetics-Practice-Resources/Practice-Guidelines.aspx>

ChopChop2, <http://chopchop.cbu.uib.no/>

ClinVar, <https://www.ncbi.nlm.nih.gov/clinvar/>

Combined Annotation Dependent Depletion (CADD), <http://cadd.gs.washington.edu>

DECIPHER, <https://decipher.sanger.ac.uk>

EMBL-EBI Expression Atlas, <https://www.ebi.ac.uk/gxa/experiments/E-ERAD-475/Results>

Ensembl, <https://www.ensembl.org/index.html>

Ensembl Variant Effect Predictor (VEP) pipeline, <https://www.ensembl.org/info/docs/tools/vep/index.html>

Exon-Intron Graphic Maker, <http://wormweb.org/exonintron>

FastQC, <http://www.bioinformatics.bbsrc.ac.uk/projects/fastqc>

Gene Cards, <http://www.genecards.org>

Gene Matcher, <http://www.genematcher.org>

Genome Aggregation Database (GnomAD), <http://gnomad.broadinstitute.org>

Genomic Evolutionary Rate Profiling – GERP, <http://mendel.stanford.edu/SidowLab/downloads/gerp/>

Human Genome Variation Society, <https://varnomen.hgvs.org>

Leiden Open Variation Database (LOVD), <https://www.lovd.nl>

Mutation Assessor, <http://mutationassessor.org/r3/>

Mutation Taster, <http://www.mutationtaster.org>

Online Mendelian Inheritance in Man, <http://www.ncbi.nlm.nih.gov/Omim>

Polyphen-2, <http://genetics.bwh.harvard.edu/pph2/>

Proteomics DB, <https://www.proteomicsdb.org>

PubMed, <http://www.ncbi.nlm.nih.gov/pubmed>

RefSeq, <https://www.ncbi.nlm.nih.gov/refseq>

SIFT, <https://sift.bii.a-star.edu.sg>

Splice AI, <https://spliceailookup.broadinstitute.org>

TIDE, <https://tide.nki.nl/>

UniProt, <https://www.uniprot.org>

UCSC Human Genome Database, <http://www.genome.ucsc.edu>

Varsome, <https://varsome.com>

- ¹Department of Neurosciences, Rehabilitation, Ophthalmology, Genetics, Maternal and Child Health, University of Genoa, Genoa, Italy
- ²Pediatric Neurology and Muscular Diseases Unit, IRCCS Istituto Giannina Gaslini, University of Genoa, 16147 Genoa, Italy
- ³Medical Genetics Unit, IRCCS Giannina Gaslini Institute, Genoa, Italy
- ⁴Stanley Manne Children's Research Institute, Ann & Robert H. Lurie Children's Hospital of Chicago, Chicago, IL 60611, USA
- ⁵CHU Nantes, Department of Medical Genetics, CHU Nantes, 9 quai Moncousu, 44093 Nantes, France
- ⁶CHU Nantes, UF of Fœtopathology and Genetics, 9 quai Moncousu, 44093 Nantes, France
- ⁷CHU de Bordeaux, Service de Génétique Médicale, F-33000, Bordeaux, France
- ⁸Department of Human Genetics, David Geffen School of Medicine, University of California Los Angeles, Los Angeles, CA 90095
- ⁹Department of Human Genetics, Hannover Medical School, 30625 Hannover, Germany
- ¹⁰CHU Nantes, Department of Anatomical Pathology, 9 quai Moncousu, 44093 Nantes, France
- ¹¹Center for Human Disease Modeling, Duke University Medical Center, Durham, NC 27701, USA
- ¹²CHU Nantes, Department of Obstetrics and Gynecology, quai 38 bd Jean Monnet, 44093, Nantes, France
- ¹³Department of Clinical Genetics, Birmingham Women's and Children's NHS Foundation Trust & Birmingham Health Partners
- ¹⁴Department of Medicine, University of Birmingham, Birmingham, UK
- ¹⁵Child Neuropsychiatry Unit, IRCCS G. Gaslini Institute, Genoa, Italy
- ¹⁶Department of Precision Medicine, University of Campania "Luigi Vanvitelli", Naples, Italy
- ¹⁷Telethon Institute of Genetics and Medicine, Pozzuoli, Italy
- ¹⁸Nantes Université, CHU de Nantes, CNRS, INSERM, l'institut du thorax, F-44000 Nantes, France
- ¹⁹Insitro, South San Francisco, CA 94080, USA
- ²⁰Stanley Center for Psychiatric Research, Broad Institute of MIT and Harvard, Cambridge, MA, USA
- ²¹Department of Pediatrics and Department of Cell and Developmental Biology, Feinberg School of Medicine, Northwestern University, Chicago, IL 60611, USA
- ²²Molecular Biology Institute, University of California Los Angeles, Los Angeles, CA 90095 USA
- ²³These authors contributed equally
- ²⁴These authors contributed equally

Abstract

Purpose: We established the genetic etiology of a syndromic neurodevelopmental condition characterized by variable cognitive impairment, recognizable facial dysmorphism, and a constellation of extra-neurological manifestations.

Methods: We performed phenotypic characterization of six participants from four unrelated families presenting with a neurodevelopmental syndrome and used exome sequencing (ES) to investigate the underlying genetic cause. To probe relevance to the neurodevelopmental phenotype and craniofacial dysmorphism, we established two- and three-dimensional human stem cell-derived neural models, and generated a stable *cachd1* zebrafish mutant on a transgenic cartilage reporter line.

Results: Affected individuals showed mild cognitive impairment, dysmorphism featuring oculo-auriculo abnormalities, and developmental defects involving genitourinary and digestive tracts. ES revealed biallelic putative loss-of-function variants in *CACHD1* segregating with disease in all pedigrees. RNA sequencing in *CACHD1*-depleted neural progenitors (NPCs) revealed abnormal expression of genes with key roles in Wnt signaling, neurodevelopment, and organ morphogenesis. *CACHD1* depletion in NPCs resulted in reduced percentages of post-mitotic neurons and enlargement of 3D neurospheres. Homozygous *cachd1* mutant larvae showed mandibular patterning defects mimicking human facial dysmorphism.

Conclusion: Our findings support the role of loss-of-function variants in *CACHD1* as the cause of a rare neurodevelopmental syndrome with facial dysmorphism and multisystem abnormalities.

INTRODUCTION

Voltage-gated calcium channels (VGCCs) act as electrical excitability transducers in neuronal, cardiac, and muscle cells by mediating Ca^{2+} influx in response to action potentials and subthreshold depolarizing signals¹. Distinct molecular subtypes of VGCCs are implicated in signal transduction in different cell types¹. This functional specialization reflects specific physiological, pharmacological, and regulatory properties of VGCC subtypes that play critical roles in hormone secretion, transmitter release, and both excitation-transcription and excitation-contraction coupling¹. Dysfunctional VGCCs increase the risk for schizophrenia, heart arrhythmias, muscle weakness, and a broad range of other disorders known as channelopathies². The physiological properties of VGCCs—and the cells in which they are expressed—are largely determined by the pore-forming $\alpha 1$ subunits, while $\alpha 1$ -interacting auxiliary β and $\alpha 2\delta$ subunits modulate cell-surface expression and trafficking^{3,4}. The importance of these subunits on VGCC physiology is well-established, but it is less clear if other subunit-interacting proteins can influence channel function and contribute to the onset of disease.

The $\alpha 2\delta$ -like cache domain containing 1 (*CACHD1*; MIM: 620144) protein forms a complex with and modulates the activity and expression of high voltage-activated N-type ($\text{Ca}_v2.2$) and low voltage-activated T-type (Ca_v3) channels^{5,6}. High levels of *CACHD1* mRNA and protein are present in the mammalian central nervous system (CNS), especially in the cerebellum, hippocampus, and thalamus⁵. At the tissue level, *CACHD1* expression overlaps the distribution of $\alpha 2\delta-3$ proteins and Ca_v3 subunits; at the subcellular level, this

protein colocalizes with Ca_v2.2 and Ca_v3 channels at the cell surface^{5,6}. Overexpression of *CACHD1* significantly increases Ca_v2.2 and Ca_v3 current density and maximal conductance, and CACHD1 is thought to exert these physiological effects by increasing cell surface expression and reducing endocytosis of these N- and T-type channels^{5,6}. Importantly, members of the $\alpha 2\delta$ protein family have putative roles in development and disease independent of VGCC modulation, suggesting that the same could be true for CACHD1⁷.

In vitro studies have nominated CACHD1 as a regulator of neural progenitor cell (NPC) proliferation and differentiation⁸, as well as neuronal presynaptic function, the latter of which is consistent with the known contributions of N-type channels to presynaptic neurotransmitter release⁹. These early reports suggest that CACHD1 plays important roles in the mammalian brain; however, the ramifications of *CACHD1* gene-disrupting variants on human health are unknown.

We assembled a cohort of six affected individuals from four unrelated families who harbor biallelic putative loss-of-function variants in *CACHD1* and present with a rare neurodevelopmental syndrome characterized by variable developmental delay, cognitive impairment, craniofacial dysmorphism, and a recurrent pattern of multisystem abnormalities. Accordingly, molecular and cellular characterization of *CACHD1*-depleted human stem cell-derived NPCs revealed disease-relevant dysregulated pathways and defects in neurogenesis. Furthermore, *cachd1*-mutant zebrafish models recapitulated the craniofacial abnormalities observed in human patients. Our results provide *in vitro* and *in vivo* evidence for a pathogenic role of biallelic *CACHD1* variants.

MATERIALS AND METHODS

Study approval and recruitment

Six individuals from four unrelated families were recruited after clinical assessment at different research centers and hospitals (Supplemental Methods). The study cohort was assembled using gene matching platforms¹⁰ and through international collaborative efforts. Detailed phenotypic information related to prenatal and developmental history, clinical evaluations, and medical imaging were provided by the referring physicians. Informed consent was collected from parents or legal guardians for genetic investigation and publication of clinical and genetic data. Approval was obtained as mentioned in the Ethics Declaration section.

Genetic analysis

Chromosomal microarray analysis (CMA) was performed in individuals #1–4 as described¹¹, and the detected rearrangements were interpreted according to DECIPHER.

ETHICS DECLARATION

This research study adheres to the principles in the Declaration of Helsinki and was approved by the medical ethical committee installed by Gaslini Children's Hospital (Comitato Etico della Regione Liguria, approval code 163/2018). Written informed consent was obtained from parents or legal guardians of all the enrolled participants for clinical testing and publication of genetic and clinical data, as well as clinical photographs. Patient privacy was always prioritized and respected during the exchange of data among researchers and clinicians.

Exome sequencing (ES) was performed on genomic DNA extracted from peripheral blood leukocytes. Parent-proband ES was performed in all participants (trios in #1–4 and duos in #5 and #6) as previously described¹¹. Additional sequencing methodology is described in the Supplemental Methods. Genetic variants were filtered for minor allele frequency (MAF) > 0.01 in genomic databases (gnomAD), presence in ClinVar, conservation (Genomic Evolutionary Rate Profiling), and predicted impact on protein structure and function. Using the Ensembl Variant Effect Predictor pipeline, several *in silico* tools were employed to predict variant pathogenicity, including Combined Annotation Dependent Depletion (GRCh37-v1.6 version), Polyphen-2, Mutation Taster, and Splice AI, as previously reported¹¹. Sanger sequencing was performed to confirm candidate variants and for parental segregation analysis. Candidate variants were classified according to the American College of Medical Genetics and Genomics and the Association for Molecular Pathology guidelines. All *CACHD1* variants are reported according to RefSeq NM_020925.4 (GenBank NC_000001.11) and HGVS recommendations. All variants were submitted to the Leiden Open Variation Database with the following accession numbers: #0000830402, #0000830403, #0000830406, #0000830407, #0000830408, and #0000830409.

Cell culture and CRISPR

Human embryonic stem cells (hESCs) were transduced with dox-inducible Ngn2 lentivirus and split every 4–5 days in mTesR media (Supplemental Methods). Transduced hESCs were then induced to NPCs using the Stem cell-derived NGN2-accelerated Progenitor (SNaP) method⁸, which were cultured in bFGF/EGF-containing maintenance media. NPCs were split weekly and plated at 120,000 cells/cm². NPCs were transduced with Cas9-lentivirus (pLX-311-Cas9 vector) followed by selection with blasticidin (10 µg/mL). NPCs were then transduced with individual lentivirus sgRNAs targeting *CACHD1* before selection with puromycin (1 µg/mL) for one week. Cells were harvested for Sanger sequencing and TIDE analysis.

RNA sequencing

RNAseq libraries were prepared with the KAPA Stranded mRNA-Seq Kit (KAPA Biosciences) and sequenced on a HiSeq 3000 (Illumina) to generate single-end 50 bp reads. FASTQ files were aligned to the human reference genome version GRCh38 and processed for DEG analysis and gene functional enrichment analysis (Supplemental Methods).

Differentiation assay

NPCs were plated for 30 days in spontaneous differentiation media before immunostaining as described in the Supplemental Methods. For each well of a 96-well plate, 4–8 fluorescent images were captured using the Cytation5 multi-mode reader (BioTek Instruments). All images were processed using the CellProfiler imaging analysis software to quantify the percentage of HuCD⁺ neurons or SOX2⁺ NPCs.

SNaP-derived neurospheres

SNaPs were dissociated in accutase and plated at 18,000 cells/well of an ultra-low attachment 96-well round bottom plate (Corning, 7007) in 150 μ L of SNaP maintenance media supplemented with Y-27632 (50 μ M). Two days later (Day 2), 75 μ L of conditioned media was removed from each well and replaced with 150 μ L of fresh SNaP maintenance media supplemented with Y-27632 (50 μ M). The following day (Day 3), 125 μ L of conditioned media was removed from each well using the “blast” technique and replaced with 150 μ L of fresh SNaP maintenance media without Y-27632¹². From Day 4 onward, 150 μ L of conditioned media was removed every other day from each well using the “blast” technique and replaced with 150 μ L of fresh SNaP maintenance media. Neurospheres were measured using the Cytation5 multi-mode reader using the 4X bright field objective.

Single-cell RNA sequencing

10X Genomics libraries from 10 pooled neurospheres were generated and sequenced on a HiSeq 4000 (Illumina). scRNA-seq datasets were analyzed using Seurat²¹³. Graph-based clustering approximated different cell groups, and t-stochastic neighborhood embedding (TSNE) analysis was used for 2D representation.

Generation and molecular characterization of *cachd1* zebrafish mutants

All studies performed in zebrafish were approved by the Institutional Animal Care and Use Committees (IACUC; Protocols A154–18-06 and IS00016405) at Duke University Medical Center and Northwestern University, respectively. To identify the *cachd1* ortholog in zebrafish, we performed a reciprocal BLAST of human CACHD1 protein (GRCh38.p13, Ensembl: ENST00000651257.2; RefSeq: NP_065976.3) against the zebrafish genome. We synthesized sgRNA using the Gene Art precision gRNA synthesis kit (Invitrogen) per manufacturer’s instructions. We estimated sgRNA efficiency using heteroduplex analysis (n=2 wildtype [WT] and n=10 injected embryos) and TOPO-TA cloning-based sequencing (n=1 WT and n=5 injected embryos; 24 clones per embryo) as described¹⁴ (Supplementary Methods). To generate stable F2 homozygous mutants (–/–), F0 mutants carrying germline *cachd1* insertion-deletions (indels) were outcrossed with WT (+/+) and then F1 heterozygous mutants (+/–) were in-crossed. To assess the expression of mutant *cachd1* mRNA, we generated F2 larvae from in-crosses of heterozygous parents (n=20 larvae per genotype; 2dpf) and performed quantitative (q)PCR assays.

Zebrafish phenotyping

We used the Vertebrate Automated Screening Technology (VAST; Union Biometrica) Bioimager platform to perform live automated imaging of anterior cartilage structures in *-1.4coll1a1:egfp* larvae as described (Supplementary Methods)¹⁵. We in-crossed genotype-matched adults (either +/+ or –/–) to generate larvae for phenotyping. Fluorescent images were assessed using ImageJ (NIH) by measuring the area surrounded by ceratohyal, palatoquadrate and Meckel’s cartilage (defined as region of interest, ROI). Statistical differences were calculated using an unpaired student’s t-test. Measurements were performed with investigators masked to genotype and repeated twice.

RESULTS

CACHD1 patients show neurodevelopmental impairment and congenital multisystem defects

Six affected individuals in four unrelated families presented with a syndromic neurodevelopmental condition featuring abnormalities in multiple organ systems (Table 1; Figure 1a–d; Supplemental Table 1; Supplemental Clinical Information). Excluding the fetal cases (#5 and #6), neurological involvement was present in all participants. A global impairment of psychomotor development was reported in individuals #3 and #4, with the latter overcoming developmental delays by the age of 2 years. The degree of cognitive impairment was generally mild. Individuals #1–3 exhibited learning disabilities leading to writing and speech impairment in early childhood. Psychomotor regression was not reported. Behavioral disturbances occurred in two participants (#1 and #2), including attention deficit hyperactivity disorder (ADHD), irritability, immature social skills, and anxiety. Mild sleep disturbances were reported in patient #2, whereas an isolated epileptic episode occurred in participant #3 at the age of 1 year. Brain magnetic resonance imaging (MRI) was normal in two of the three tested participants (#1 and #3), while nonspecific findings were observed in individual #4 (Table 1).

All cases displayed dysmorphic facial features that included hypo- or hypertrichosis, medially sparse eyebrows, and bulbous nose tip (Figure 1c). Minor dysmorphic features were reported in individuals #1 (widely spaced nipples) and #2 (nipple skin tag). Variable ear abnormalities were observed in five of six individuals, and consisted of microtia, ear displacement or malrotation, hypo-dysplasia of the outer ear, preauricular skin tags, and uplifted earlobes. Four participants (#1–4) showed variable congenital eye anomalies, ranging from developmental defects (e.g., obstruction of the nasolacrimal ducts and bilateral glaucoma with buphthalmos) to benign tumors of choristomatous nature, such as epibulbar dermoid (individual #3) and lipodermoid (individual #1).

Congenital anomalies in different organ systems were common (Table 1; Supplemental Table 1). Five participants showed genitourinary abnormalities, of which three had renal involvement (unilateral renal agenesis in individual #2; uretero-renal obstruction leading to hydronephrosis in individuals #5 and #6); three cases presented with genital malformations, such as hypospadias (individual #2), cryptorchidism associated with inguinal hernia (individual #3), and abnormal enlargement of the clitoris associated with a distal skin tag (individual #4). Congenital malformations of the digestive tract (CMDTs) were diagnosed in three cases. Two participants (individuals #1 and #2) showed a similar pattern of anorectal malformations (ARM) consisting of anal displacement or atresia combined with rectoperineal fistula, whereas esophageal atresia was observed in participant #5. Musculoskeletal features were less common and included scoliosis (individual #1), foot malformation (individuals #1 and #4), and Perthes disease (individual #2). Cardiac involvement consisted of patent ductus arteriosus (PDA) and patent foramen ovale (PFO) in individual #2, and peripheral pulmonary artery stenosis (PAS) and ventricular septal defect (VSD) in individual #4. No rhythm abnormalities were detected.

Identification and *in silico* analysis of *CACHD1* variants

We investigated each affected individual for copy number variants (CNVs) and single nucleotide variants (SNVs). CMA was uninformative for individuals #1–5; individual #5 had a normal karyotype, and individual #6 did not undergo chromosomal assessment (Supplemental Table 1). However, ES led to the identification of biallelic putative loss-of-function variants in *CACHD1* (GenBank ID: NM_020925.4) segregating with disease in all pedigrees: c.1783–1G>A and c.2387+1G>A in family I; c.261+2T>C and c.648delC; p.(Ile217Serfs*13) in family II; homozygous c.274dup; p.(Ile92Asnfs*52) in family III; and c.277C>T; p.(Arg93*) and c.460C>T; p.(Arg154*) in family IV (Figure 1a–b; Table 1; Supplemental Table 1).

All variants are rare (allele frequency ranging from 0 to 0.0000402), are absent in the homozygous state in gnomAD, and are predicted to be pathogenic by multiple *in silico* tools (Table 1; Supplemental Table 2). The variants are dispersed across the *CACHD1* locus, though four of the six changes (two frameshift and two stop gain variants) cluster in the region from intron 2 to exon 6. All variants are predicted to result in the loss of protein function either through nonsense-mediated mRNA decay (NMD) or the formation of an unstable truncated transcript. According to gnomAD, the probability of being loss-of-function intolerant (pLi) of *CACHD1* is 0. However, the Loss-of-function Observed/Expected Upper-bound Fraction (LOEUF) score is 0.31 and the Z score for pLoF variants is 4.279, leading to a 100% probability of intolerance to recessive loss-of-function variants (<https://varsome.com/gene/hg38/cachd1>). Furthermore, the screening of our in-house database of 6,000 control exomes did not identify loss-of-function genotypes comparable to those observed in the reported individuals (Supplemental Table 3). Thus, our sequencing data indicates that mutations in *CACHD1* result in the clinical symptoms observed in this patient cohort.

CACHD1 depletion disrupts neurogenesis in human cells

It is unclear how *CACHD1* ablation from early neural cells could affect the mechanisms underlying brain development. Fetal neurogenesis relies on normal NPC proliferation and differentiation dynamics. To test the role of *CACHD1* in neurogenesis, we depleted *CACHD1* expression in H1 human embryonic stem cell (hESC)-derived NPCs that were generated using the SNaP protocol⁸ (Figure 2a). Two *CACHD1*-targeting sgRNAs were delivered separately to assess the reproducibility of effects, while one non-targeting (NT) sgRNA was used as a control. TIDE analysis revealed high mosaicism of over 95% editing efficiency for both guide RNAs (Supplemental Figure 1a–b).

We allowed NPCs to spontaneously differentiate for 30 days to measure differentiation potential. *CACHD1*-edited cell lines showed reduced percentages of HuCD⁺ post-mitotic neurons, suggesting deficits in neuronal differentiation (Figure 2b). Measurements of NPC content revealed a modest but significant increase in SOX2⁺ progenitors in *CACHD1* sgRNA^{#2} conditions relative to controls, while sgRNA^{#1} targeted cells showed a non-significant trend towards an increase of NPCs (Figure 2c). These findings corroborate recent analysis of *CACHD1*-depleted human cerebral organoids⁸ and further suggest that

CACHD1-disrupted cells have an impaired ability to transition from proliferative NPCs to post-mitotic neurons.

Genome-wide CRISPR-Cas9 screening in 2D cultures previously identified *CACHD1* as a regulator of NPC proliferation⁸. To test the impact of *CACHD1* depletion under conditions of relevant cytoarchitecture and cell-type diversity¹⁶, we developed a protocol for generating 3D neurospheres from SNaPs (Figure 2d). Lightsheet imaging of day 7 unedited neurospheres immunostained with the NPC marker phospho-Vimentin (phVim) and the neurite marker MAP2 showed that both progenitors and early neuronal cells were present (Figure 2e). We further characterized the cellular composition of SNaP-derived neurospheres through scRNA-seq. Seven days post-neurosphere formation, we found 12.5% of the cells expressed transcripts enriched in post-mitotic neurons such as *ELAVL4* and *STMN2* (Group 4) while the remaining were either *MKI67*⁺ mitotic cells (Group 1, 34.3%) or progenitor cells that expressed *PAX6* and *SOX2* (Group 2, 28.2%; Supplemental Figure 2a–e). A subset of the quiescent state progenitors (Group 3, 25.0%) expressed genes that are typically upregulated under hypoxic conditions, such as *BNIP3* and *SLC2A1*. Together, these findings support the utility of our SNaP-derived neurospheres for 3D modeling of NPC proliferation.

We produced neurospheres from *CACHD1*-depleted and NT sgRNA control SNaPs and found *CACHD1* sgRNA #1 and #2 neurospheres were significantly larger than controls (Figure 2f–g) indicative of a hyperproliferative NPC phenotype. Collectively, our results indicate that *CACHD1* plays a critical role in NPC cellular functions that occur during the earliest stages of brain development, and its genetic ablation could contribute to profound neurodevelopmental disorders.

Loss of *CACHD1* alters neurodevelopmental gene expression programs

To understand the molecular mechanisms affected by *CACHD1* loss, we harvested NPCs for bulk RNA sequencing analysis. We detected 432 significant differentially expressed genes (DEGs) between the control and *CACHD1* sgRNA^{#1}, and 1,924 DEGs between the control and sgRNA^{#2} (Figure 3a). Overall, 382 dysregulated genes (180 upregulated and 202 downregulated) were shared between the two datasets (Figure 3b–c). Enrichment analysis of gene ontology (GO) terms was conducted on these DEG lists to identify dysfunctional biological functions.

Genes involved in broad neurobiological processes such as nervous system development (GO:0007399), neurogenesis (GO:0022008), synapse structure and activity (GO:0050803) were dysregulated in depleted cells (Figure 3d–e; Supplemental Data File 1). Key neurodevelopmental genes showed dramatic changes in expression, including *SIX3* ($\log_2FC = -4.62$), *HES1* (-1.74), *CRABP2* (1.83), *WNT5B* (1.99), and *NEUROD4* (2.51). Interestingly, our list of 382 DEGs showed significant overlap with high confidence autism ($p=7.30e-04$, odds ratio=2.1) and developmental delay risk genes ($p=7.20e-04$, odds ratio=3.5) such as *CNTNAP2*, *GRIN2B*, and *PTEN*, indicating potential biological convergence with established neurodevelopmental disorder risk factors.

Next, we set out to better understand the molecular contributors to the defective neurogenesis phenotypes we observed. Downregulated genes were enriched for such GO

terms as regulation of neurogenesis (GO:0050767), neuron differentiation (GO:0045664), and negative regulation of cell population proliferation (GO:0008285), while upregulated genes were involved in neuroblast proliferation (GO:0007405), neuron differentiation, and cell division (GO:0051302). The downregulation of negative regulators of growth, including *PTEN* ($\log_2FC=-0.45$), *MAPK21* (-0.67), and *CDKN1C* (-0.77) could explain the hyperproliferative phenotype. *CDKN1C* downregulation is also of interest given this gene's role in promoting terminal differentiation of NPCs¹⁷. The reduced expression of differentiation-stimulating genes like *CDKN1C*, *SOX4*, and *SOX11* could explain the lower differentiation potential of *CACHD1*-depleted cells.

Our data also highlight a potential role for *CACHD1* in the Wnt signaling pathway, which regulates the balance between NPC proliferation and differentiation¹⁸. Downregulated genes were enriched for negative regulators of Wnt (GO:0030178), while upregulated genes were enriched for positive regulators (GO:0090263). These reciprocal effects suggest that the Wnt pathway may be overactivated in *CACHD1*-depleted cells, which is known to enhance proliferation and impair differentiation of NPCs¹⁹.

Beyond neurodevelopment, we detected abnormalities in other processes that may be relevant to our patient cohort. For example, our DEGs were enriched for genes involved in development of the head (GO:0060322), heart (GO:0007507), kidney (GO:0001822), skeletal system (GO:0001501), and urogenital system (GO:0001655; Figure 3e). Our analysis also revealed defects in molecular processes involved in pancreatic function (GO:0003310) and formation of amyloid-beta plaques (GO:1902003), the latter of which plays a central role in Alzheimer's disease pathology. Collectively, these results suggest that disruption of *CACHD1* expression impacts essential developmental processes and nominate gene expression programs that may underlie *CACHD1*-associated defects in neuronal and non-neuronal tissues.

Homozygous *cachd1* mutant zebrafish larvae recapitulate human craniofacial dysmorphism

In vitro human models are a powerful tool for studying the mechanisms underlying disease, but are not able to recapitulate complex systems and structures, such as craniofacial development. To further establish the physiological relevance of *CACHD1* dysfunction to human disease, we generated a zebrafish model. Reciprocal BLAST with human *CACHD1* protein identified a single *cachd1* ortholog in zebrafish (87% identity, 94% similarity; Figure 4a). *cachd1* has robust mRNA levels detectable from the zygote stage, which persist in whole larval RNAseq data until at least 5 dpf^{20,21}. We targeted exon 9 of the *cachd1* locus by injecting sgRNA and Cas9 protein into the cell of 1-cell stage embryos. Further molecular characterization of F0 mosaic mutants showed moderate mosaicism (47% mosaicism with insertion/deletion events proximal to the PAM site in F0s, n=5 embryos per condition, 24 clones per embryo). F0 animals were outcrossed with WT (+/+) mates, and we identified an F0 founder carrying a 16 bp indel (p.(Phe452Leufs*3); Figure 4b). We in-crossed F1 heterozygous (+/-) mutants to generate an F2 generation for subsequent molecular validation. To confirm efficient ablation of *cachd1* transcript in homozygous mutants (-/-), we performed qPCR on total RNA obtained from genotype-matched 2 dpf

larvae (genotypes: *cachd1*^{+/+}, *cachd1*^{+/-}, *cachd1*^{-/-}); we observed a significant reduction (~70–80%) in *cachd1* RNA levels in homozygotes compared to WT siblings ($p < 0.0001$ versus WT; Figure 4c).

Facial dysmorphisms are morphological features in humans bearing biallelic *CACHD1* variants (Table 1; Supplemental Table 1; Figure 1c), prompting us to evaluate orthologous structures in zebrafish mutant larvae according to our *in vivo* imaging paradigm^{22,23} (Figure 4d). Using F2 adult siblings, we in-crossed either WT or homozygous mutant animals harboring the *-1.4coll1a1:egfp* transgenic cartilage reporter and simultaneously performed live lateral bright field imaging and ventral imaging of fluorescent signal in F3 larvae at 3 dpf. We observed no gross morphological abnormalities (Figure 4e, top). However, quantification of the mandibular area encompassed by ceratohyal, palatoquadrate and Meckel's cartilage showed a significant reduction in the ROI area in *cachd1*^{-/-} compared to *cachd1*^{+/+} larvae ($p < 0.0001$; Figure 4e–f). These data suggest that dysfunction of *cachd1* leads to cartilage patterning defects.

DISCUSSION

Defects in calcium channels have been implicated in several syndromic neurodevelopmental conditions²⁴. VGCCs play crucial roles during neurodevelopment, including neural cell survival, neurite extension, and radial migration²⁴. Pathogenic variants in genes encoding the $\alpha 1$ subunits of VGCCs result in heterogeneous neurodevelopmental features with or without other syndromic conditions²⁵. Here, we identified six individuals harboring seven putative loss-of-function variants in *CACHD1*—which encodes a protein that interacts directly with VGCCs—presenting with a rare neurodevelopmental syndromic condition characterized by developmental delay, learning disabilities, facial dysmorphism, and extra-neurological manifestations featuring oculo-auricular abnormalities, genitourinary defects, and congenital malformations. *In vitro* human neural models of *CACHD1* depletion displayed dysregulated Wnt signaling, which is in alignment with a recent report that nominates *CACHD1* as a Wnt regulator in the developing brain²⁶; it remains to be determined if Wnt dysfunction directly contributes to the altered NPC proliferation and differentiation we observed. Zebrafish *cachd1* mutants displayed cartilage patterning defects, which is a proxy for human facial dysmorphic features. Collectively, our *in vitro* and *in vivo* findings reflect the developmental defects observed in human patients, nominating *CACHD1* as a contributor to human brain and craniofacial development.

The *CACHD1*-associated cellular defects we observed align with the established role of VGCCs in neurogenesis^{29,30}, and the clinical manifestations of *CACHD1* variants—such as psychomotor development delay (2 of 4 cases), cognitive disability (3 of 4 cases), and neuropsychiatric features (2 of 4 cases)—are shared with calcium channelopathies and hint at potential converging disease biology^{31,32}. For example, Timothy Syndrome is caused by pathogenic variants in *CACNA1C*, which encodes the $\alpha 1C$ subunit of $Ca_v1.2$. This rare condition is characterized by neurodevelopmental delay, autism, and epilepsy, as well as syndactyly, prolonged QT interval, variable congenital heart defects, and facial dysmorphisms^{27,32}. Similar neurodevelopmental and psychiatric features have also been associated with *CACNA1G* ($Ca_v3.1$) variants, as have variable craniofacial anomalies and

skeletal defects^{28,33,34}. Abnormal CACHD1-mediated regulation of these channels could potentially contribute to the neuropsychiatric symptoms observed in our patients.

Historically, investigations of VGCCs and their effectors have focused on their physiological relevance to excitable cells that can fire action potentials; their contribution to the development and function of non-excitable cells has received limited attention^{35,36}.

CACNA1C and *CACNA1G* variants play causal roles in craniofacial defects, exemplifying a developmental role for VGCCs in non-excitable tissues^{27,28,32}. Deleterious variants in ion channel genes contribute to the morphological development and function of non-excitable cells in various animal models, and can result in congenital structural abnormalities³⁷.

For example, altered Ca_v1.2 channel activity leads to defects in jaw development in mice and zebrafish³⁸. Accordingly, our *cachd1* zebrafish mutants displayed cartilage patterning defects, and our RNA-seq analysis of *in vitro* human NPCs found dysregulation of transcripts involved in head and skeletal system development. Thus, the *CACHD1* human and animal models we describe could serve as important systems for further elucidation of the roles of VGCCs in non-excitable cell morphogenesis. Future studies are required to elucidate the impact of *CACHD1* dysfunction on critical craniofacial processes, such as neural crest cell formation and migration.

Some of the extra-neurological features observed in our patients overlap with oculo-auriculo-vertebral spectrum (OAVS; also known as Goldenhar syndrome), a rare condition characterized by malformations of the ears, eyes, and spine (Supplemental Figure 3). CNVs in different genetic loci have been identified in some patients, but the etiology of OAVS remains elusive⁴⁰. *CACHD1* has not been linked to this disorder, but it should be noted that OAVS minimal diagnostic criteria include features observed in our cohort such as microtia (small external ear), facial asymmetry due to hemifacial microsomia (i.e., one half of the face does not develop fully), and epibulbar dermoids/lipodermoids (benign growths in the eye). In mice, the loss of *Cachd1* disturbs Ca²⁺ homeostasis in the endolymph of the inner ear, leading to secondary membranous labyrinth dilation and audio-vestibular dysfunction⁴¹. Although hearing loss and balance impairment were not observed in our patients, it is possible that mild defects could be detected through specific tests, such as video head impulse test, Computerized Dynamic Visual Activity, high-resolution computed tomography, and MRI. Subsequent studies could investigate the potential involvement of *CACHD1* variants in the genetic susceptibility of OAVS and inner ear dysfunction.

CACHD1 may regulate key aspects of neurodevelopment independent of the modulation of VGCC activity⁴², as CACHD1-like $\alpha 2\delta$ isoforms are known to regulate synaptic function, GABA_A receptor abundance, and axonal wiring in a non-VGCC-dependent manner^{7,43,44}. Furthermore, protein products formed after CACHD1 cleavage by γ -secretase and the beta-site APP cleaving enzyme 1 (BACE1)—which is an essential catalyzer of the first step of pathogenic amyloid beta (A β) peptide generation in Alzheimer's disease—modulate signal transduction and gene expression⁴⁵.

CACHD1 has also been suggested in the pathogenesis of complex human conditions not observed in our patient cohort. Specifically, *CACHD1* may contribute to the susceptibility to diabetes mellitus (DM) type 1 and has been implicated in the hepatocarcinogenesis

associated with DM and Non-Alcoholic Steatohepatitis (NASH)^{46,47}. It is tempting to speculate that an abnormal transcriptional regulatory function may contribute to at least some of the extra-neurological developmental defects observed in our patients.

We employed ES to investigate the etiology of neurodevelopmental symptoms observed in our cohort and identified biallelic variants in *CACHD1* as the potential cause. While some LoF *CACHD1* variants may be observed in healthy controls in gnomAD, these changes never occur *in trans* in the same individual. *CACHD1* has a low LOEUF score (0.31) and high Z score for pLoF variants (4.279), suggesting intolerance to loss of function. Together with the results obtained from our functional studies, these data support the biallelic loss of *CACHD1* as the cause of the novel neurodevelopmental syndrome observed in our patients. We acknowledge that the co-occurrence of variants with milder functional impact in modifier genes or non-coding regions may influence the phenotype expressivity of monogenic neurodevelopmental disorders, and that thorough genomic analysis may be helpful to detect these co-occurring variants. Though we were unable to investigate the whole genomes of our study's participants, future broader genomic approaches could further dissect the genetic aspects of *CACHD1*-related disease.

In summary, our data expand the spectrum of human disorders related to VGCC function and suggest that *CACHD1* participates in the refinement of cognitive function and morphogenetic processes in several organ systems.

Supplementary Material

Refer to Web version on PubMed Central for supplementary material.

ACKNOWLEDGEMENTS

We are grateful to the patients and families who participated in this investigation. We sincerely thank Jill A. Rosenfeld for the valuable cooperation and support. We also acknowledge the Telethon Undiagnosed Disease Program (TUDP) for technical and scientific support.

FUNDING STATEMENT

M.F.W. is supported by the NIMH/NIH (R00MH119327). E.E.D. is supported by funds from the NICHD/NIH (R01HD105868) and NIMH/NIH (R01MH106826). E.E.D. is the Ann Marie and Francis Klocke, MD Research Scholar.

DATA AVAILABILITY

The authors declare that all data generated or analyzed during this study and supporting the findings of the study are available within the paper and its supplementary information files. Genomic data included in the study are available in the Leiden Open Variation Database (LOVD) at <https://databases.lovd.nl/shared/variants/CACHD1>.

REFERENCES

1. Catterall WA (2011). Voltage-gated calcium channels. *Cold Spring Harb. Perspect. Biol.* 3, a003947. [PubMed: 21746798]

2. Zamponi GW, Striessnig J, Koschak A, and Dolphin AC (2015). The Physiology, Pathology, and Pharmacology of Voltage-Gated Calcium Channels and Their Future Therapeutic Potential. *Pharmacol. Rev.* 67, 821–870. [PubMed: 26362469]
3. Gurnett CA, De Waard M, and Campbell KP (1996). Dual Function of the Voltage-Dependent Ca²⁺ Channel α 2 δ Subunit in Current Stimulation and Subunit Interaction. *Neuron* 16, 431–440. [PubMed: 8789958]
4. Dolphin AC (2012). Calcium channel auxiliary α 2 δ and β subunits: trafficking and one step beyond. *Nat. Rev. Neurosci.* 13, 542–555. [PubMed: 22805911]
5. Cottrell GS, Soubrane CH, Hounshell JA, Lin H, Owenson V, Rigby M, Cox PJ, Barker BS, Ottolini M, Ince S, et al. (2018). CACHD1 is an α 2 δ -like protein that modulates Cav3 voltage-gated calcium channel activity. *Journal of Neuroscience* 38, 9186–9201. [PubMed: 30181139]
6. Dahimene S, Page KM, Kadurin I, Ferron L, Ho DY, Powell GT, Pratt WS, Wilson SW, and Dolphin AC (2018). The α 2 δ -like Protein Cachd1 Increases N-type Calcium Currents and Cell Surface Expression and Competes with α 2 δ -1. *Cell Rep.* 25, 1610–1621.e5. [PubMed: 30404013]
7. Ablinger C, Geisler SM, Stanika RI, Klein CT, and Obermair GJ (2020). Neuronal α 2 δ proteins and brain disorders. *Pflugers Arch.* 472, 845–863. [PubMed: 32607809]
8. Wells MF, Nemesh J, Ghosh S, Mitchell J, Salick MR, Mello CJ, Meyer D, Pietilainen O, Piccioni F, Guss EJ, et al. (2023). Natural variation in gene expression and viral susceptibility revealed by neural progenitor cell villages. *Cell Stem Cell*, 1–21. [PubMed: 36608673]
9. Ablinger C, Eibl C, Geisler SM, Campiglio M, Stephens GJ, Missler M, and Obermair GJ (2022). α 2 δ -4 and Cachd1 Proteins Are Regulators of Presynaptic Functions. *Int. J. Mol. Sci.* 23. 10.3390/ijms23179885.
10. Sobreira N, Schiettecatte F, Valle D, and Hamosh A (2015). GeneMatcher: a matching tool for connecting investigators with an interest in the same gene. *Hum. Mutat.* 36, 928–930. [PubMed: 26220891]
11. Scala M, Nishikawa M, Ito H, Tabata H, Khan T, Accogli A, Davids L, Ruiz A, Chiurazzi P, Cericola G, et al. (2022). Variant-specific changes in RAC3 function disrupt corticogenesis in neurodevelopmental phenotypes. *Brain* 145, 3308–3327. [PubMed: 35851598]
12. Salick MR, Wells MF, Eggan K, and Kaykas A (2017). Modelling Zika Virus Infection of the Developing Human Brain In Vitro Using Stem Cell Derived Cerebral Organoids. *J. Vis. Exp.* 10.3791/56404.
13. Butler A, Hoffman P, Smibert P, Papalexi E, and Satija R (2018). Integrating single-cell transcriptomic data across different conditions, technologies, and species. *Nat. Biotechnol.* 36, 411–420. [PubMed: 29608179]
14. Khan TN, Khan K, Sadeghpour A, Reynolds H, Perilla Y, McDonald MT, Gallentine WB, Baig SM, Task Force for Neonatal Genomics, Davis EE, et al. (2019). Mutations in NCAPG2 Cause a Severe Neurodevelopmental Syndrome that Expands the Phenotypic Spectrum of Condensinopathies. *Am. J. Hum. Genet.* 104, 94–111. [PubMed: 30609410]
15. Lee Y-R, Khan K, Armfield-Uhas K, Srikanth S, Thompson NA, Pardo M, Yu L, Norris JW, Peng Y, Gripp KW, et al. (2020). Mutations in FAM50A suggest that Armfield XLID syndrome is a spliceosomopathy. *Nat. Commun.* 11, 3698. [PubMed: 32703943]
16. Sun N, Meng X, Liu Y, Song D, Jiang C, and Cai J (2021). Applications of brain organoids in neurodevelopment and neurological diseases. *J. Biomed. Sci.* 28, 30. [PubMed: 33888112]
17. Lozano-Ureña A, Lázaro-Carot L, Jiménez-Villalba E, Montalbán-Loro R, Mateos-White I, Duart-Abadía P, Martínez-Gurrea I, Nakayama KI, Fariñas I, Kirstein M, et al. (2023). IGF2 interacts with the imprinted gene Cdkn1c to promote terminal differentiation of neural stem cells. *Development* 150. 10.1242/dev.200563.
18. Alkailani MI, Aittaleb M, and Tissir F (2022). WNT signaling at the intersection between neurogenesis and brain tumorigenesis. *Front. Mol. Neurosci.* 15, 1017568. [PubMed: 36267699]
19. Pei Y, Brun SN, Markant SL, Lento W, Gibson P, Taketo MM, Giovannini M, Gilbertson RJ, and Wechsler-Reya RJ (2012). WNT signaling increases proliferation and impairs differentiation of stem cells in the developing cerebellum. *Development* 139, 1724–1733. [PubMed: 22461560]

20. White RJ, Collins JE, Sealy IM, Wali N, Dooley CM, Digby Z, Stemple DL, Murphy DN, Billis K, Hourlier T, et al. (2017). A high-resolution mRNA expression time course of embryonic development in zebrafish. *Elife* 6. 10.7554/eLife.30860.
21. Papatheodorou I, Fonseca NA, Keays M, Tang YA, Barrera E, Bazant W, Burke M, Füllgrabe A, Fuentes AM-P, George N, et al. (2018). Expression Atlas: gene and protein expression across multiple studies and organisms. *Nucleic Acids Res.* 46, D246–D251. [PubMed: 29165655]
22. Kürty S, Besnard T, Ebstein F, Khan TN, Gambin T, Douglas J, Bacino CA, Craigen WJ, Sanders SJ, Lehmann A, et al. (2017). De Novo Disruption of the Proteasome Regulatory Subunit PSMD12 Causes a Syndromic Neurodevelopmental Disorder. *The American Journal of Human Genetics* 100, 352–363. 10.1016/j.ajhg.2017.01.003. [PubMed: 28132691]
23. Ishibashi M, Ang SL, Shiota K, Nakanishi S, Kageyama R, and Guillemot F (1995). Targeted disruption of mammalian hairy and Enhancer of split homolog-1 (HES-1) leads to up-regulation of neural helix-loop-helix factors, premature neurogenesis, and severe neural tube defects. *Genes & Development* 9, 3136–3148. 10.1101/gad.9.24.3136. [PubMed: 8543157]
24. Heyes S, Pratt WS, Rees E, Dahimene S, Ferron L, Owen MJ, and Dolphin AC (2015). Genetic disruption of voltage-gated calcium channels in psychiatric and neurological disorders. *Prog. Neurobiol.* 134, 36–54. [PubMed: 26386135]
25. Zamponi GW, and Weiss N (2022). Voltage-Gated Calcium Channels (Springer Nature).
26. Powell GT, Faro A, Zhao Y, Stickney H, Novellademunt L, Henriques P, Gestri G, White ER, Ren J, Lu W, et al. (2022). *Cachd1* is a novel Frizzled- and LRP6-interacting protein required for neurons to acquire left-right asymmetric character. *bioRxiv*. 10.1101/2022.05.16.492129.
27. Bauer R, Timothy KW, and Golden A (2021). Update on the Molecular Genetics of Timothy Syndrome. *Frontiers in Pediatrics* 9. 10.3389/fped.2021.668546.
28. Chemin J, Siquier-Pernet K, Nicouleau M, Barcia G, Ahmad A, Medina-Cano D, Hanein S, Altin N, Hubert L, Bole-Feysot C, et al. (2018). De novo mutation screening in childhood-onset cerebellar atrophy identifies gain-of-function mutations in the CACNA1G calcium channel gene. *Brain* 141, 1998–2013. [PubMed: 29878067]
29. Nigussie F, Huang P-S, Lukauskis K, Bawa B, Moussa E, and Abbott LC (2016). Neural cell proliferation and survival in the hippocampus of adult CaV 2.1 calcium ion channel mutant mice. *Brain Res.* 1650, 162–171. [PubMed: 27581393]
30. Lepski G, Jannes CE, Nikkhah G, and Bischofberger J (2013). cAMP promotes the differentiation of neural progenitor cells in vitro via modulation of voltage-gated calcium channels. *Front. Cell. Neurosci.* 7, 155. [PubMed: 24065885]
31. Kessi M, Chen B, Peng J, Yan F, Yang L, and Yin F (2021). Calcium channelopathies and intellectual disability: a systematic review. *Orphanet J. Rare Dis.* 16, 219. [PubMed: 33985586]
32. Splawski I, Timothy KW, Sharpe LM, Decher N, Kumar P, Bloise R, Napolitano C, Schwartz PJ, Joseph RM, Condouris K, et al. (2004). CaV1.2 Calcium Channel Dysfunction Causes a Multisystem Disorder Including Arrhythmia and Autism. *Cell* 119, 19–31. [PubMed: 15454078]
33. Singh T, Neale BM, Daly MJ, and Consortium, on B. of T.S.E.M.-A. (schema) (2020). Exome sequencing identifies rare coding variants in 10 genes which confer substantial risk for schizophrenia. *medRxiv*, 2020.09.18.20192815.
34. Berecki G, Helbig KL, Ware TL, Grinton B, Skraban CM, Marsh ED, Berkovic SF, and Petrou S (2020). Novel Missense CACNA1G Mutations Associated with Infantile-Onset Developmental and Epileptic Encephalopathy. *Int. J. Mol. Sci.* 21. 10.3390/ijms21176333.
35. Pitt GS, Matsui M, and Cao C (2021). Voltage-Gated Calcium Channels in Nonexcitable Tissues. *Annu. Rev. Physiol.* 83, 183–203. [PubMed: 33106102]
36. Kaestner L, Wang X, Hertz L, and Bernhardt I (2018). Voltage-Activated Ion Channels in Non-excitable Cells—A Viewpoint Regarding Their Physiological Justification. *Front. Physiol.* 9. 10.3389/fphys.2018.00450.
37. Ozekin YH, Isner T, and Bates EA (2020). Ion Channel Contributions to Morphological Development: Insights From the Role of Kir2.1 in Bone Development. *Frontiers in Molecular Neuroscience* 13. 10.3389/fnmol.2020.00099.

38. Ramachandran KV, Hennessey JA, Barnett AS, Yin X, Stadt HA, Foster E, Shah RA, Yazawa M, Dolmetsch RE, Kirby ML, et al. (2013). Calcium influx through L-type CaV1.2 Ca²⁺ channels regulates mandibular development. *J. Clin. Invest.* 123, 1638–1646. [PubMed: 23549079]
39. Beleza-Meireles A, Clayton-Smith J, Saraiva JM, and Tassabehji M (2014). Oculo-auriculo-vertebral spectrum: a review of the literature and genetic update. *J. Med. Genet.* 51, 635–645. [PubMed: 25118188]
40. Bragagnolo S, Colovati MES, Souza MZ, Dantas AG, F de Soares MF, Melaragno MI, and Perez AB (2018). Clinical and cytogenomic findings in OAV spectrum. *Am. J. Med. Genet. A* 176, 638–648. [PubMed: 29368383]
41. Tian C, Johnson KR, Lett JM, Voss R, Salt AN, Hartsock JJ, Steyger PS, and Ohlemiller KK (2021). CACHD1-deficient mice exhibit hearing and balance deficits associated with a disruption of calcium homeostasis in the inner ear. *Hear. Res.* 409, 108327. [PubMed: 34388681]
42. Andrade A, Brennecke A, Mallat S, Brown J, Gomez-Rivadeneira J, Czepiel N, and Londrigan L (2019). Genetic associations between voltage-gated calcium channels and psychiatric disorders. *Int. J. Mol. Sci.* 20, 3537. [PubMed: 31331039]
43. Eroglu C, Allen NJ, Susman MW, O'Rourke NA, Park CY, Ozkan E, Chakraborty C, Mulinyawe SB, Annis DS, Huberman AD, et al. (2009). Gabapentin receptor alpha2delta-1 is a neuronal thrombospondin receptor responsible for excitatory CNS synaptogenesis. *Cell* 139, 380–392. [PubMed: 19818485]
44. Schöpf CL, Ablinger C, Geisler SM, Stanika RI, Campiglio M, Kaufmann WA, Nimmervoll B, Schlick B, Brockhaus J, Missler M, et al. (2021). Presynaptic $\alpha 2\delta$ subunits are key organizers of glutamatergic synapses. *Proc. Natl. Acad. Sci. U. S. A.* 118, e1920827118. [PubMed: 33782113]
45. Rudan Njavro J, Klotz J, Dislich B, Wanngren J, Shmueli MD, Herber J, Kuhn P-H, Kumar R, Koeglsperger T, Conrad M, et al. (2020). Mouse brain proteomics establishes MDGA1 and CACHD1 as in vivo substrates of the Alzheimer protease BACE1. *FASEB J.* 34, 2465–2482. [PubMed: 31908000]
46. Kakehashi A, Chariyakornkul A, Suzuki S, Khuanphram N, Tatsumi K, Yamano S, Fujioka M, Gi M, Wongpoomchai R, and Wanibuchi H (2021). Cache domain containing 1 is a novel marker of non-alcoholic steatohepatitis-associated hepatocarcinogenesis. *Cancers (Basel)* 13, 1216. [PubMed: 33802238]
47. Rassi DM, Junta CM, Fachin AL, Sandrin-Garcia P, Mello S, Silva GL, Evangelista AF, Magalhães DA, Wastowski IJ, Crispim JO, et al. (2008). Gene expression profiles stratified according to type 1 diabetes mellitus susceptibility regions. *Ann. N. Y. Acad. Sci.* 1150, 282–289. [PubMed: 19120314]

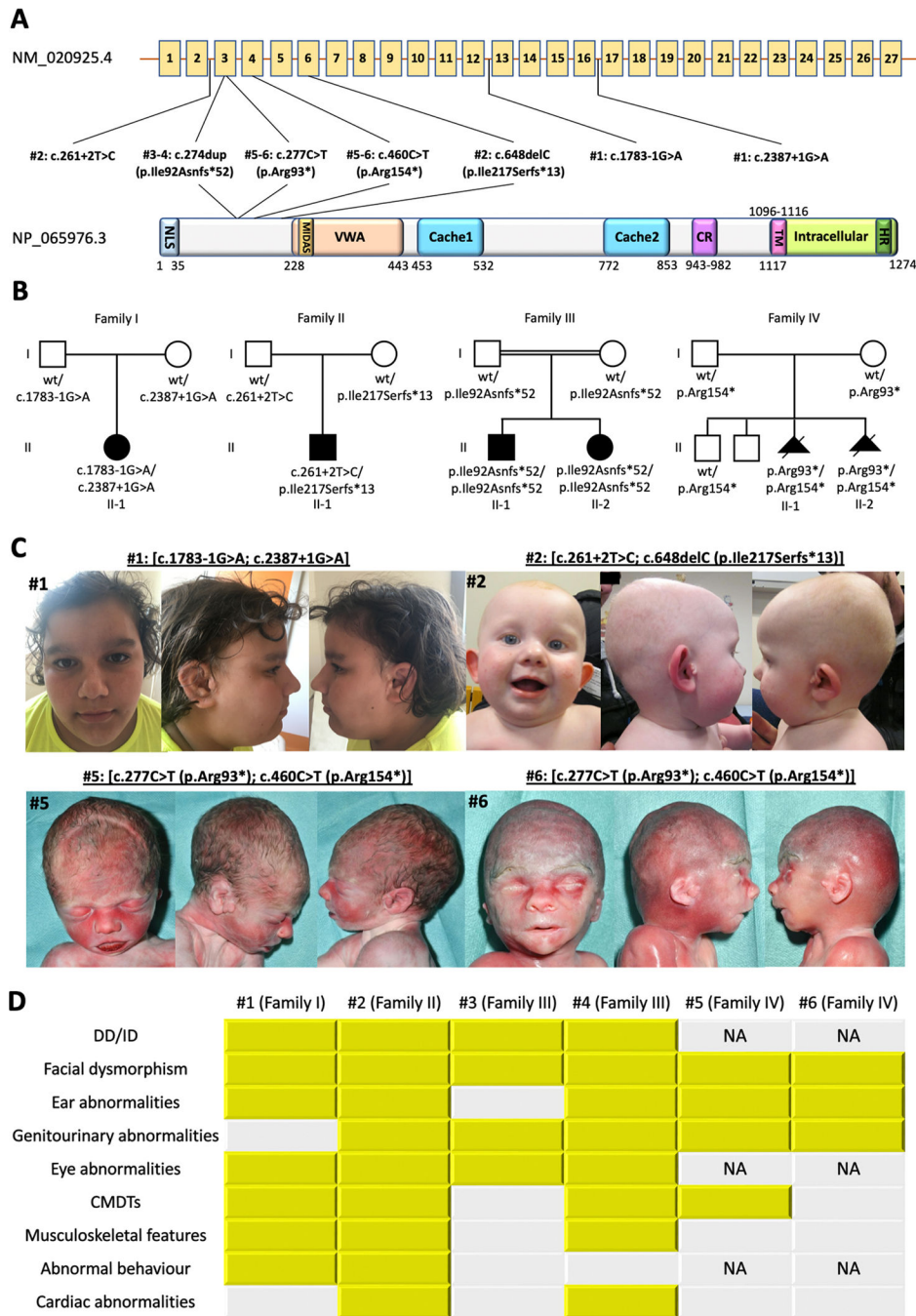


Figure 1. Genetic and clinical aspects of affected individuals harboring *CACHD1* variants. (A) Location of *CACHD1* variants in relation to exonic location (top); and domain structure (bottom; GenBank: NM_020925.4, NP_065976.3). *CACHD1* consists of an exofacial N-terminus, a von Willebrand factor A (VWA) domain, two bacterial chemosensory-like cache domains, a short hydrophobic transmembrane domain, and an intracellular C-terminus. Exonic variants affect exons 3, 4, and 6. Intronic variants localize in introns 2, 12, and 16. Most variants affect the early portion of the gene, predicted to lead to premature transcription termination and putative nonsense-mediated mRNA decay. Numbers under

the protein schematic indicate amino acid numbers. Abbreviations are as follows: Cache, Ca^{2+} channel and chemotaxis receptor; CR, cysteine rich; HR, histidine rich; MIDAS, metal ion-dependent adhesion site; NLS, nuclear localization signal; TM, transmembrane domain. Locations of domains are approximate based on data from www.Uniprot.org. **(B)** Pedigrees of the reported families with the segregation patterns of *CACHDI* variants. Open shapes, unaffected individuals; filled shapes, affected individuals; square, male; circle, female, triangle, pregnancy not carried to term; wt, wild type. **(C)** Clinical photographs. Individual #1 at 13 years shows sparse hair, medially sparse eyebrows, a pit on the left cheek, and small and posteriorly rotated ears with preauricular tags, underdeveloped crus of the helix, and uplifted earlobes. Individual #2 at 1 year shows bilateral preauricular skin tags associated with overfolding of the superior helices. Individuals #5 (31+5 weeks) and #6 (21+5 weeks) show long and thick eyebrows, periorbital rings, palpebral edema, low-set ears with dysplastic outer ear and bilateral preauricular skin tags, and macroglossia. **(D)** Graph summarizing the distribution of the most common clinical features (present in at least two cases) in the reported cohort. Abbreviations: CMDTs, congenital malformations of the digestive tract; DD, developmental delay; ID, intellectual disability; NA, not applicable.

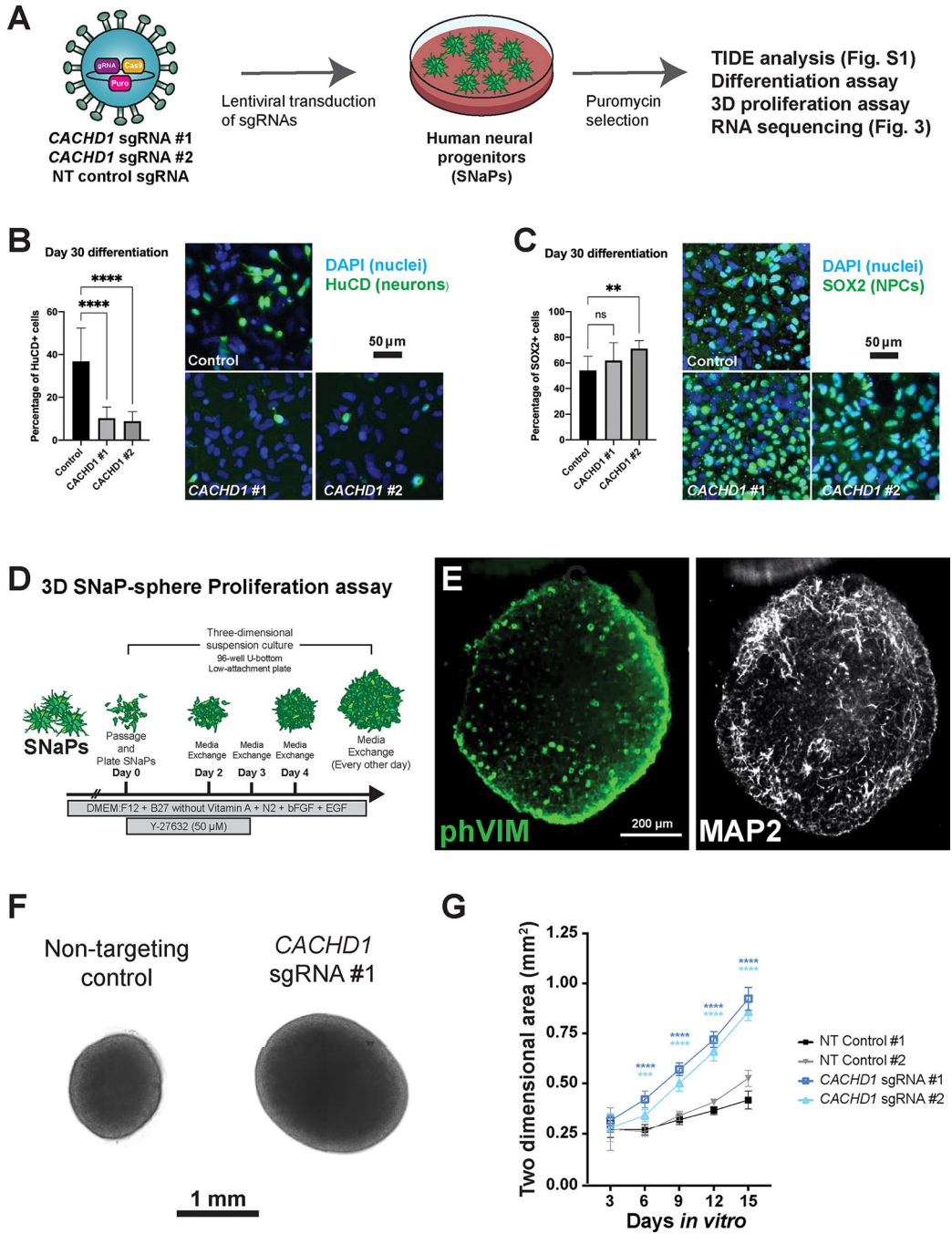


Figure 2. *CACHD1* depletion alters NPC proliferation and differentiation.

(A) Schematic describing the workflow of NPC cellular. (B) Quantification of the percentage of HuCD⁺ post-mitotic neurons in Day 30 differentiation cultures from control and *CACHD1*-edited SNaP lines. Representative images depict nuclei in blue and HuCD in green. Scale bar = 50 μ m. (C) Quantification of the percentage of SOX2⁺ NPCs in Day 30 differentiation cultures from control and *CACHD1*-edited SNaP lines. Representative images depict nuclei in blue and SOX2 in green. Scale bar = 50 μ m. (D) Schematic describing the production of three-dimensional (3D) neurospheres derived from two-

dimensional SNaP cultures. (E) Lightsheet imaging of a Day 7 SNaP-neurosphere stained with phospho-Vimentin (NPC marker) and MAP2 (neurite marker). (F) Representative bright field images of control and *CACHD1*-edited neurospheres at day 15 post-plating. Scale bar = 1 mm. (G) Quantification of Panel F. Data are represented as mean \pm S.D.

Author Manuscript

Author Manuscript

Author Manuscript

Author Manuscript

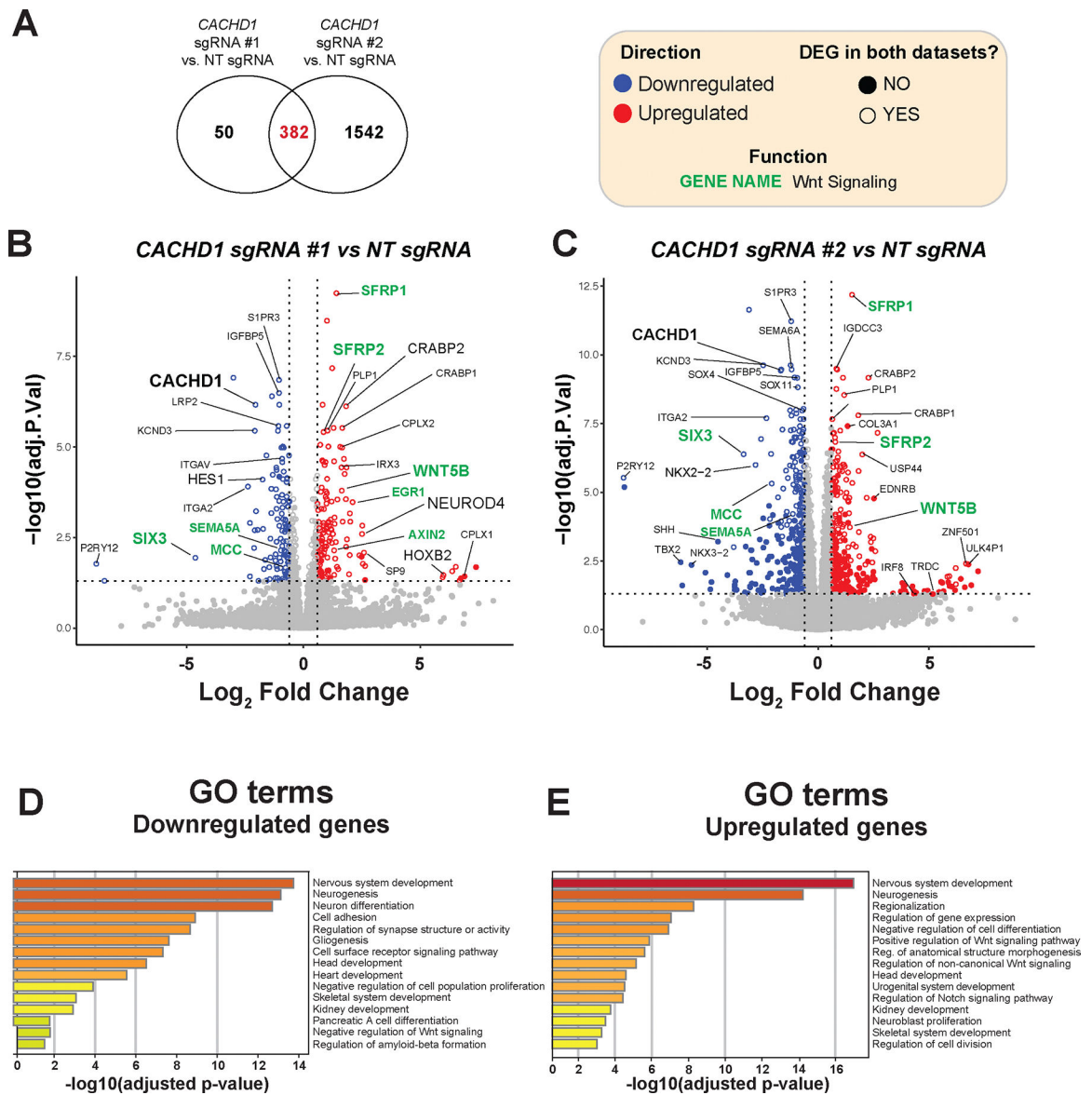


Figure 3. Genetic ablation of *CACHD1* impacts expression of key neurodevelopmental genes and signaling pathways.

(A) Venn diagram depicting the overlap of differentially expressed genes (DEGs) between the two *CACHD1*-depleted NPC lines. (B-C) Volcano plots of DEGs, comparing each *CACHD1*-depleted line to NT control. Open circles reflect DEGs consistent in both *CACHD1*-depleted lines relative to NT control. Positive mean log₂ fold change (FC) refers to genes that are upregulated in *CACHD1*-edited cells. Statistical significance is defined as Benjamini-Hochberg adjusted p-values <0.05. Vertical dashed lines represent log₂FC = 0.6 (FC ~ 1.5 fold), while horizontal dashed lines represent the adjusted p-value threshold of p <0.05. DEGs that pass both the significance and FC thresholds are colored in red (upregulated) or blue (downregulated). Genes in green are known Wnt pathway genes. (D-E) Gene ontology (GO) term analysis of 382 DEGs; (D) downregulated and (E) upregulated genes in *CACHD1*-depleted lines.

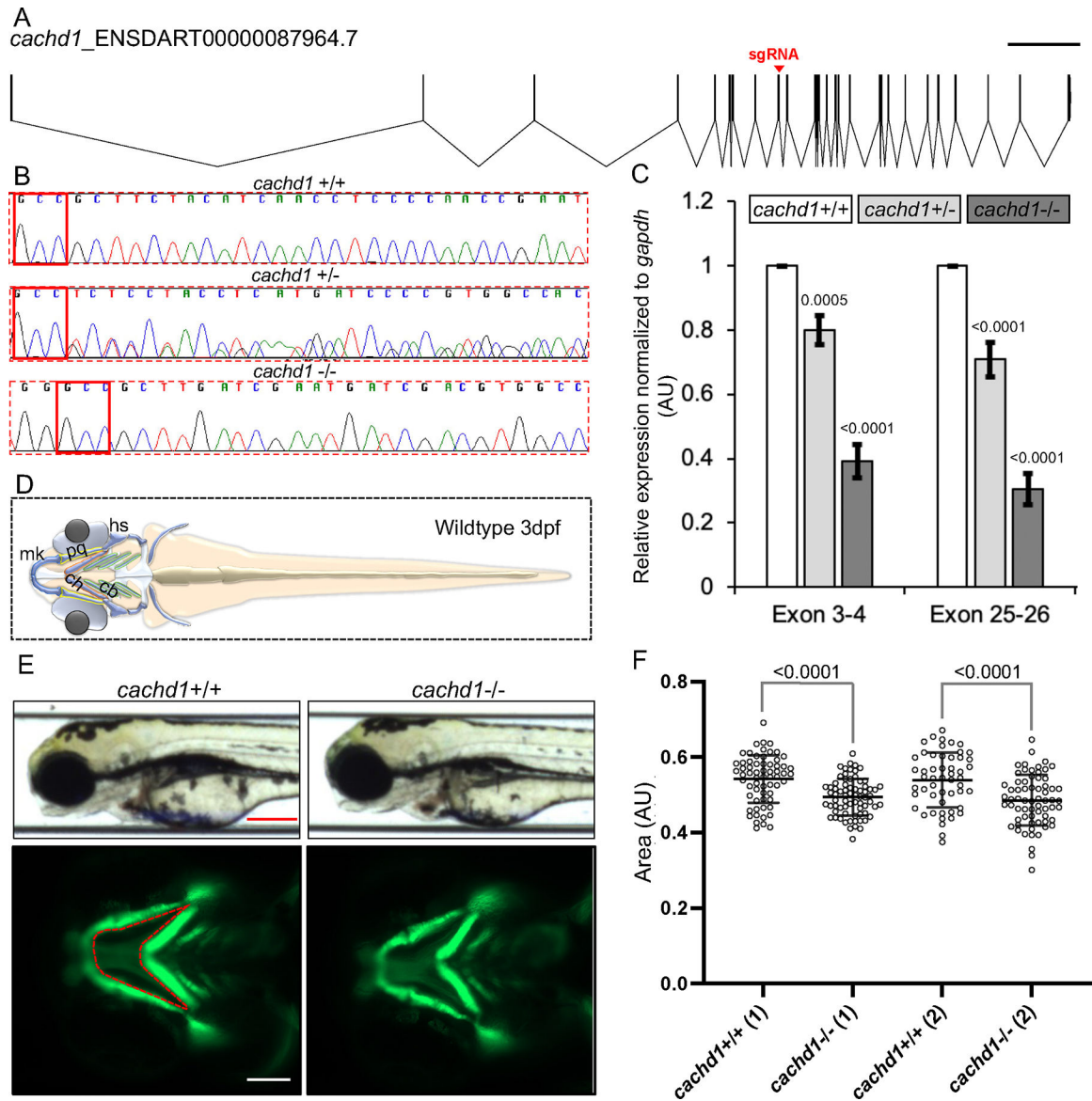


Figure 4. Ablation of zebrafish *cachd1* by CRISPR-Cas9 results in craniofacial abnormalities.

(A) Schematic of zebrafish *cachd1* transcript (GRCz11, Ensembl transcript ID: ENSDART00000087964.7) generated by Exon-Intron Graphic Maker (<http://wormweb.org/exonintron>). The sgRNA target site on exon 9 is indicated by a red triangle. Scale bar, 10 kb. (B) Representative sequence chromatograms of *cachd1* +/+ (wild type), *cachd1* +/- (heterozygous mutant), *cachd1* -/- (homozygous mutant) are shown. Protospacer adjacent motif (PAM) is indicated by a red box for each chromatogram. Mutants harbor a 16 bp deletion (19 bp deletion and 3 bp insertion) that results in a frameshift and putative protein truncation (p.Phe452LeufsTer3). (C) Bar graph showing relative mRNA expression of *cachd1* in genotype-matched 2 day post-fertilization (dpf) larvae generated from F1 in-crosses. n=20 per batch, three technical replicates per experiment, eight biological replicates (One way ANOVA; Tukey's multiple comparisons test). Tails were used for genotyping while RNA was extracted from the matched heads for quantitative PCR

analysis. Relative expression was normalized to *gapdh* and statistical differences were calculated using One way ANOVA [$F(5, 42) = 50.39$; $P \text{ value} < 0.0001$]; Tukey's multiple comparisons test's p-values for mutants versus $+/+$ are indicated above each bar. Error bars represent standard error of the mean. **(D)** Schematic of 3 dpf zebrafish larva showing a ventral view of craniofacial cartilage structures. Abbreviations: Meckel's cartilage (mk, blue), palatoquadrate (pq, yellow), ceratohyal (ch, orange), hyosymplectic (hs, gray), ceratobranchial (cb, green). **(E)** Representative images of *-1.4coll1a1:egfp,cachd1* larvae imaged live at 3 dpf. Top: Bright field lateral images of wild type and homozygous mutants. Scale bar, 200 μm . Bottom: Fluorescent ventral images of wild type and homozygous mutants. Region of interest (ROI) area, as outlined in red and bordered by ch, pq and mk, was measured to detect statistical differences. Scale bar, 100 μm . **(F)** Quantification of ROI indicated in panel **(E)**; AU, arbitrary units. Statistical differences were calculated using an unpaired t-test ($n=50-70$ larvae per condition, repeated). Biological replicates (1 and 2 as indicated in x-axis labels) were obtained from different parental pairs with the investigator was masked to the experimental conditions. Regardless of their parental genotype, all embryos obtained were morphologically similar and no animal was excluded from imaging and quantification. Error bars represent standard deviation of the mean.

Table 1.Genetic and clinical features of *CACHD1* participants.

| | #1 (family I) | #2 (family II) | #3 (family III) | #4 (family III) | #5 (family IV) | #6 (family IV) |
|---|--|--|-----------------------------------|-----------------------------|--|--|
| Age, gender | 13.5 y, F | 8.6 y, M | 8 y, M | 2 y, F | 31+5 we, M | 22+2 we, M |
| <i>CACHD1</i> variant(s) (NM_020925.4) | [c.1783-1G>A; c.2387+1G>A] | [c.261+2T>C; c.648del (p.Ile217Serfs*13)] | c.274dup (p.Ile92Asnfs*52) | c.274dup (p.Ile92Asnfs*52) | [c.277C>T (p.Arg93*); c.460C>T (p.Arg154*)] | [c.277C>T (p.Arg93*); c.460C>T (p.Arg154*)] |
| Inheritance | Comp het | Comp het | Hom | Hom | Comp het | Comp het |
| Allele frequency (gnomAD, v3.1.2) | 0; 0 | 0.00000657; 0 | 0 | 0 | 0.00000401; 0.0000402 | 0.00000401; 0.0000402 |
| ACMG/AMP class (criteria) | Pathogenic (PVS1, PM2, PP3); Pathogenic (PVS1, PM2, PP3) | Pathogenic (PVS1, PM2, PP3); Pathogenic (PVS1, PM2, PP3) | Pathogenic (PVS1, PM2, PP3) | Pathogenic (PVS1, PM2, PP3) | Pathogenic (PVS1, PM2, PP3); VUS - Likely pathogenic (PVS1, PP3) | Pathogenic (PVS1, PM2, PP3); VUS - Likely pathogenic (PVS1, PP3) |
| Psychomotor delay (HP:0001263) | No | No | Yes | Yes | NA | NA |
| Cognitive impairment (HP:0100543) | Yes, mild | Yes, mild | Yes, mild | No | NA | NA |
| Seizures (HP:0001250) | No | No | No | Yes | NA | NA |
| Neuropsychiatric features (HP:0000708) | Anxiety; irritability; ADHD; poor social skills | Anxiety; sleep disorder | No | No | NA | NA |
| Facial dysmorphism (HP:0001999) | Yes | Yes | Yes | Yes | Yes | Yes |
| Ear abnormalities (HP:0000598) | Microtia, posterior rotation, preauricular tags, helix hypoplasia, uplifted earlobes | Overfolding of superior helices, preauricular skin tags | No | Preauricular skin tags | Displacement, dysplastic outer ear, preauricular skin tags | Displacement, dysplastic outer ear, preauricular skin tags |
| Hearing loss (HP:0000365) | No | No | No | No | NA | NA |
| Eye abnormalities (HP:0000478) | Nasolacrimal duct obstruction; strabismus; epibulbar lipodermoid | Strabismus, blepharitis | Peters anomaly, epibulbar dermoid | Coloboma | NA | NA |
| CMDTs (HP:0025031) | ARM with anal displacement rectoperineal fistula | ARM with anal atresia and recto-urethral fistula | No | ARM | Esophageal atresia (Vogt Type 2) | No |
| Genital abnormalities (HP:0000078) | No | Hypospadias | Cryptorchidism, inguinal hernia | Clitoromegaly | No | No |
| Renal defects (HP:0000077) | No | Unilateral renal agenesis | No | No | Hydronephrosis due to urethro- | Hydronephrosis due to urethro- |

| | #1 (family I) | #2 (family II) | #3 (family III) | #4 (family III) | #5 (family IV) renal obstruction | #6 (family IV) renal obstruction |
|--|---|--|-----------------|---|--|--|
| Cardiac abnormalities (HP:0001627) | No | PDA and PFO | No | Pulmonary stenosis, VSD | No | No |
| Abnormal ECG (HP:0003115) | No | No | No | No | No | No |
| Musculoskeletal features (HP:0033127) | Scoliosis, short neck, broad halluces, flat feet | Bilateral Perthes disease, proximal thumbs insertion | No | Left forefoot adduction | No | No |
| Other clinical features | Trigonocephaly (HP:0000243); obesity (HP:0001513); hemifacial microsomia (HP:0011332) | No | No | Relative enlargement of neurocranium (HP:0002683) | Hypertrichosis (HP:0000998), accessory spleen (HP:0001747) | Hypertrichosis (HP:0000998), accessory spleen (HP:0001747) |
| Brain MRI | Normal | NA | Normal | Nonspecific findings | NA | NA |

ACMG/AMP, American College of Medical Genetics and Genomics/Association for Molecular Pathology; ADHD, attention deficit-hyperactivity disorder; ARM, anorectal malformation; CMDT, congenital malformations of the digestive tract; Comp het, compound heterozygous; ECG, electrocardiogram; Hom, homozygous; NA, not applicable; PDA, patent ductus arteriosus; PFO, patent foramen ovale; PM, pathogenic moderate; PP, pathogenic supporting; PVS, pathogenic very strong; VSD, ventricular septal defect; we, weeks; y, years.